

Metal–Insulator Transition and Crystal Structure of $\text{La}_{1-x}\text{Sr}_x\text{CoO}_3$ as Functions of Sr-Content, Temperature, and Oxygen Partial Pressure

Atsushi Mineshige,^{*,1} Masafumi Kobune,^{*} Satoshi Fujii,^{*} Zempachi Ogumi,[†] Minoru Inaba,[†] Takeshi Yao,[‡] and Kenji Kikuchi[§]

^{*}Department of Applied Chemistry, Himeji Institute of Technology, Himeji, Hyogo 671-2201, Japan; [†]Department of Energy and Hydrocarbon Chemistry, Graduate School of Engineering, Kyoto University, Sakyo-ku, Kyoto 606-8501, Japan; [‡]Department of Fundamental Energy Science, Graduate School of Energy Science, Kyoto University, Sakyo-ku, Kyoto 606-8501, Japan; and [§]Department of Materials Science, The University of Shiga Prefecture, Hikone, Shiga 522-0057, Japan

Received March 27, 1998; in revised form September 30, 1998; accepted October 1, 1998

Electrical properties of $\text{La}_{1-x}\text{Sr}_x\text{CoO}_3$ (LSC) change with variations in Sr content, temperature, and oxygen partial pressure. With a change in each variable, LSC showed metal–insulator transition (MIT). The changes in electrical properties of LSC were correlated here with those of its crystal structure. The variations of crystallographic parameters such as the length of a -axis, the rhombohedral angle, the Co–O distance, and the Co–O–Co angle (θ) were precisely determined by powder X-ray Rietveld analysis. Of these, the variation of θ described most consistently the variation of conduction state, metallic or insulating, of LSC. The Co–O–Co angle increased whenever the conduction state changed from insulating to metallic by changing each variable, Sr content, temperature, and oxygen partial pressure. In addition, MIT took place at a critical Co–O–Co angle of ca. 165° in each case. It was concluded that the transition from insulator to metal is caused by the closing of the charge transfer band gap, induced by broadening of the electronic bandwidths of the Co-3d and O-2p bands with an expansion of the Co–O–Co angle. © 1999 Academic Press

1. INTRODUCTION

Perovskite oxide $\text{La}_{1-x}\text{Sr}_x\text{CoO}_3$ (LSC) is a mixed ionic and electronic conductor and has been widely investigated for use in various high-temperature electrochemical devices, such as solid oxide fuel cells (1–5) or oxygen permeation membranes (6–8). Furthermore, LSC has attracted the attention of many workers because it exhibits metal–insulator transition (MIT) by Sr doping [MIT(x)] or temperature rise [MIT(T)]. Although a number of studies on the electrical properties of LSC have been reported since the 1950s (9–18), there has been little research to correlate MIT of this system with a subtle change in its crystal structure except our previous work (19). In the previous

study, we investigated precisely the change in the crystal structure of LSC by Sr doping using a powder X-ray Rietveld method (19). We observed that a contraction of the Co–O distance and an expansion of the Co–O–Co angle appear discontinuously at ca. $x \sim 0.25$ in $\text{La}_{1-x}\text{Sr}_x\text{CoO}_3$, at which the conduction state changed from insulating (semiconducting) to metallic. These results suggested that the mechanism of MIT can be discussed from a crystallographic viewpoint.

In high-temperature electrochemical devices, LSC is used at different oxygen partial pressure [$P(\text{O}_2)$] and temperatures (T). Since both variables significantly affect the electrical conductivity of LSC (16), it is very important to clarify the behavior of the electrical conductivity and to correlate it with its crystal structure over a wide range of T or $P(\text{O}_2)$. In the present work, we precisely determined crystallographic parameters of LSC at different T and $P(\text{O}_2)$ using a powder X-ray Rietveld method. The changes to crystallographic parameters were correlated with those to electrical properties. The mechanism of MIT observed in this system was discussed in relation to crystallographic changes.

2. EXPERIMENTAL

$\text{La}_{1-x}\text{Sr}_x\text{CoO}_3$ ($x = 0.0$ and 0.3) samples were prepared by a conventional solid phase reaction. Mixtures of La_2O_3 (Wako Pure Chemicals), CoCO_3 (Hayashi Pure Chemicals), and SrCO_3 (Hayashi Pure Chemicals) powders of desired ratios were pressed into pellets and fired at 1473 K for 12 h in air. No evidence of impurity phases could be found in X-ray diffraction (XRD) patterns of the samples. The relative density of each sample was higher than 85%. The ratio of cations was confirmed by inductively coupled plasma (ICP) spectrometry, and it was almost in agreement with that of the starting mixture.

¹To whom correspondence should be addressed.

To investigate the effect of temperature, a sintered sample of LaCoO_3 [$\text{LSC}(x = 0.0)$] was ground finely, and its XRD patterns were obtained at elevated temperatures (773–993 K) in air using a Rigaku RAD-3TR system. $\text{MoK}\alpha$ radiation was used as an X-ray source. The accelerating voltage and current were 40 kV and 35 mA, respectively. Data were collected in the range $9^\circ \leq 2\theta \leq 35^\circ$ with a step width of 0.01° and an integration time of 12 s. The crystal structure of the sample at each temperature was refined using the powder X-ray Rietveld program RIEVEC (19, 20). Rhombohedral $R\bar{3}c$ was used as a space group (11) and the occupation number of oxygen atoms was assumed as unity over the experimental temperature range (16). The Rietveld profile refinement gave a precise fitting result at each temperature with a reliability factor (R_{wp}) less than 7%. Interatomic Co–O distances and Co–O–Co angles were calculated from oxygen coordinates obtained by Rietveld analysis.

To examine the effect of $P(\text{O}_2)$, $\text{La}_{0.7}\text{Sr}_{0.3}\text{CoO}_3$ [$\text{LSC}(x = 0.3)$] samples were used. The samples were annealed at temperatures in the 1073–1473 K range in argon/oxygen gas mixtures of desired ratios ($1 \times 10^{-3} \leq P(\text{O}_2)/\text{atm} \leq 2 \times 10^{-1}$). After the samples had annealed sufficiently, the electrical conductivity was measured by a standard d.c. four-probe method on cooling at $100\text{--}500 \text{ K h}^{-1}$ from the annealing temperature to room temperature (RT). $P(\text{O}_2)$ was kept constant during cooling. The annealed samples were ground and then subject to XRD measurements. XRD patterns were obtained at RT using a Rigaku RAD-B system. $\text{MoK}\alpha$ radiation was used as an X-ray source, and the accelerating voltage and current were 45 kV and 40 mA, respectively. Data were collected in the range $9^\circ \leq 2\theta \leq 60^\circ$ with a step width of 0.01° and an integration time of 15 s. The crystal structure of the samples was refined by RIEVEC. The R_{wp} value was less than 8% in each case. The mean valence of cobalt n in each annealed sample was determined by iodometry (9), and the resulting occupation number of oxygen atoms $[(3 - \delta)/3]$ was taken into consideration for Rietveld refinement.

3. RESULTS

3.1. Effect of Temperature on Electrical Properties and Lattice Parameters

We previously studied the effect of Sr content on the crystal structure and electrical conductivity (σ) of LSC ($0.0 \leq x \leq 0.7$) (19). Figure 1 shows temperature dependencies of σ in air obtained in the previous study. Although LSC has a high oxide ion conductivity as well as an electronic one, the electronic transference number is nearly unity (16, 21, 22), and hence σ shown in Fig. 1 can be regarded as the electronic one. LSC samples with $0.25 \leq x \leq 0.7$ showed metallic behavior ($\partial\sigma/\partial T < 0$) over the whole temperature range studied, whereas samples with

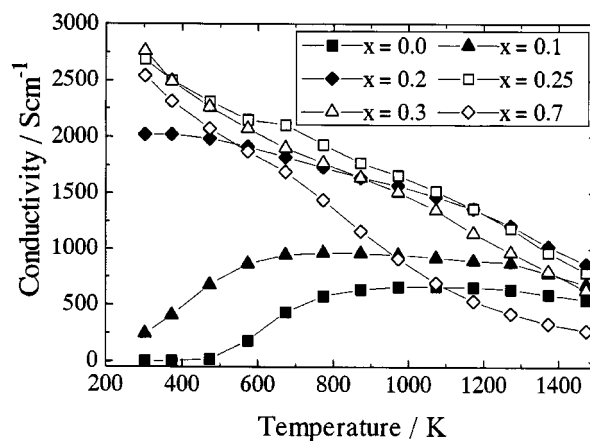


FIG. 1. Temperature dependencies of electrical conductivity of $\text{La}_{1-x}\text{Sr}_x\text{CoO}_3$ ($0.0 \leq x \leq 0.7$) samples measured in air.

$x \leq 0.20$ showed insulating (semiconducting) behavior ($\partial\sigma/\partial T > 0$) in the vicinity of RT. These facts showed that MIT of $\text{La}_{1-x}\text{Sr}_x\text{CoO}_3$ at RT [MIT(x)] is located at $x \sim 0.25$.

LSC crystallizes in either cubic or rhombohedral structure depending on Sr content and temperature. The crystal structure of LSC is shown in Fig. 2, where a_r and α_r refer to the length of a -axis and the rhombohedral angle, respectively, of the rhombohedral unit cell, and a_h and c_h refer to the

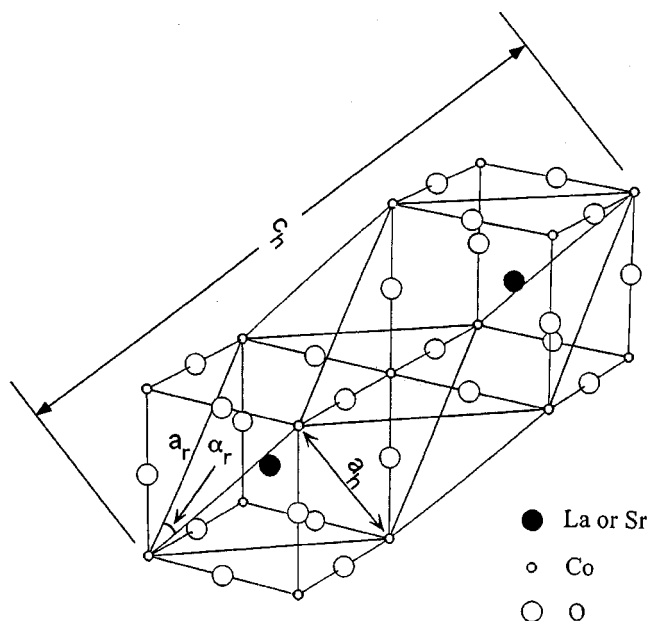


FIG. 2. Crystal structure of $\text{La}_{1-x}\text{Sr}_x\text{CoO}_3$ perovskite. Symbols a_r and α_r denote the a -axis length and the rhombohedral angle of the rhombohedral unit cell, respectively. Symbols a_h and c_h denote the a -axis and c -axis lengths of the hexagonal unit cell, respectively. In the cubic region ($0.55 \leq x \leq 0.7$ at RT), α_r is equal to 60° , whereas it is greater than 60° in the rhombohedral region.

length of a -axis and c -axis, respectively, of the hexagonal unit cell. In the rhombohedral region, the ratio c_h/a_h decreases gradually with increasing α_r . The α_r value of LSC ($x = 0.0$) is about 60.8° at RT (11, 14, 16, 19). It decreases with an increase in x or T , and becomes 60° (cubic region) at $x = 0.55$ (at RT) (11, 16, 19) or at $T \sim 1673$ K (at $x = 0.0$) (16).

As shown in Fig. 1, the electrical conductivity of LSC ($x = 0.0$) increased with T up to ca. 1000 K, and then decreased with T ; that is, it showed metallic behavior at temperatures above 1000 K. This indicates that MIT of LSC ($x = 0.0$) by temperature rise [MIT(T)] is located at $T \sim 1000$ K in air. Figure 3 shows XRD patterns of LSC ($x = 0.0$) at elevated temperatures. No significant changes (e.g., change in symmetry) were observed except for slight peak shifts in the whole temperature range tested. The temperature dependencies of a_r and α_r of LSC ($x = 0.0$) are shown in Fig. 4. The lattice constant a_r increased monotonically with increasing T to 943 K due to thermal expansion. The expansion coefficient of lattice obtained by XRD was $24.0 \times 10^{-6} \text{ K}^{-1}$ ($\text{RT} \leq T \leq 943 \text{ K}$), which was in good agreement with a reported thermal expansion coefficient of LSC ($x = 0.0$) [$23.7 \times 10^{-6} \text{ K}^{-1}$, $\text{RT} \leq T \leq 1373 \text{ K}$ (23)]. The linear increase in a_r with T was suppressed at $T \sim 973$ K, where a_r discontinuously changed. It should be noted that this temperature coincides with that of MIT(T) as shown in Fig. 1. Above 973 K, a_r increased again linearly with an increase in temperature, where LSC ($x = 0.0$) showed metallic behavior as displayed in Fig. 1. Although the crystal structure of LSC at elevated temperatures has been studied so far by XRD (10) and neutron diffraction (14), such a discontinuous change at MIT(T) has not been reported. A similar discontinuous change was observed for the rhombohedral angle α_r at $T \sim 973$ K.

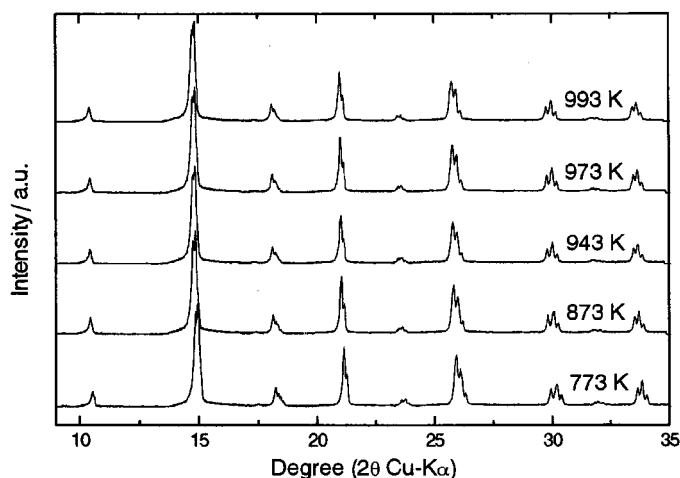


FIG. 3. XRD patterns of LaCoO_3 in the temperature range $773 \leq T/\text{K} \leq 993$.

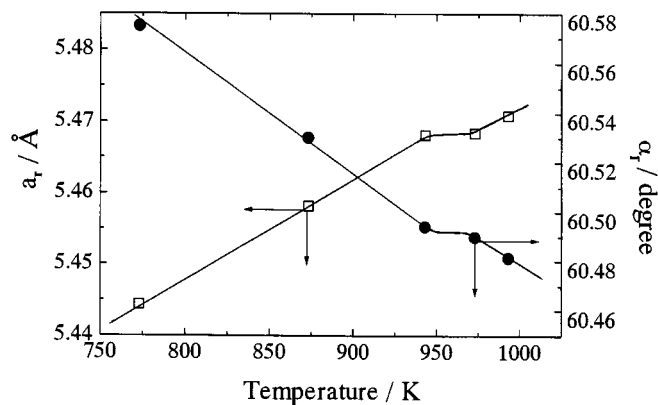


FIG. 4. Variations of (□) a -axis length a_r and (●) rhombohedral angle α_r in the rhombohedral system of LaCoO_3 at elevated temperatures.

3.2. Effect of $P(\text{O}_2)$ on Electrical Properties and Lattice Parameters

Since MIT(x) of LSC at RT occurs at $x \sim 0.25$ as shown in Fig. 1, the electrical property of LSC ($x = 0.3$) in air should be located just at the metallic side of the boundary between metal and insulator. Hence its conduction state is expected to be easily changed to insulating by a subtle change of other variables such as $P(\text{O}_2)$. Thus we chose LSC ($x = 0.3$) samples to examine the effects of $P(\text{O}_2)$ on their electrical properties and lattice parameters. Table 1 shows the mean valences of cobalt (n) of LSC ($x = 0.3$) after annealed at elevated temperatures in various $P(\text{O}_2)$ gas mixtures. Oxygen nonstoichiometry ($3 - \delta$ in $\text{La}_{0.7}\text{Sr}_{0.3}\text{CoO}_{3-\delta}$) is also listed. The excess negative charge introduced by Sr doping to LaCoO_3 is compensated either by creation of holes, that is, oxidation of Co^{3+} to Co^{4+} , or by creation of oxygen vacancies. If the excess charge is compensated only by oxidation of Co^{3+} to Co^{4+} , the n value of LSC ($x = 0.3$) should be 3.3 according to electroneutrality. Values of n less than 3.3 imply the presence of oxygen vacancies. After annealing at $T = 1473$ K and $P(\text{O}_2) = 1 \times 10^{-2}$ atm (sample 8), an n value less than 3 was obtained, which resulted from the decomposition of the sample. While LSC ($x = 0.3$) decomposed at $P(\text{O}_2) \leq 10^{-2}$ atm (at 1473 K), or $P(\text{O}_2) \leq 4 \times 10^{-3}$ atm (at 1273 K), no decomposition product formed in the present experimental $P(\text{O}_2)$ range at 1073 K.

Figure 5a shows the effect of $P(\text{O}_2)$ on the electrical conductivity of LSC ($x = 0.3$) (samples 3–5) annealed at 1073 K under atmospheres in the range $1 \times 10^{-3} \leq P(\text{O}_2)/\text{atm} \leq 4 \times 10^{-3}$. After annealing at $P(\text{O}_2) \geq 2 \times 10^{-3}$ atm, LSC ($x = 0.3$) showed metallic behavior over the whole temperature range, whereas after annealing at $P(\text{O}_2) = 1 \times 10^{-3}$ atm, the conducting state changed from metallic to insulating at 473 K upon cooling. These facts indicate that the conduction state of LSC is affected by

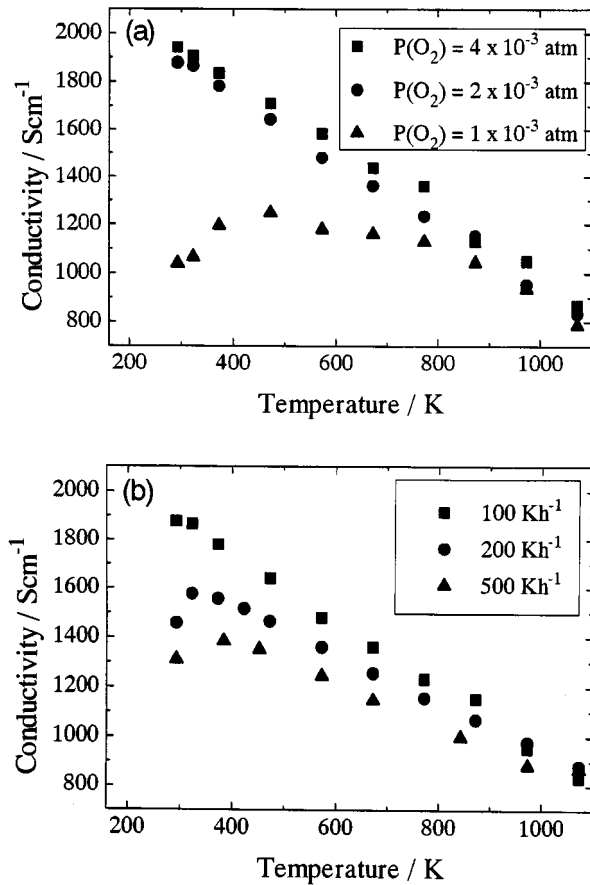


FIG. 5. Temperature dependencies of electrical conductivity of $\text{La}_{0.7}\text{Sr}_{0.3}\text{CoO}_3$ measured on cooling after annealed at 1073 K under various $P(\text{O}_2)$ atmospheres (a) cooled at 100 K h^{-1} and (b) cooled at various rates after annealing at $P(\text{O}_2) = 2 \times 10^{-3} \text{ atm}$.

$P(\text{O}_2)$ [MIT(P)] as well. In the case of LSC ($x = 0.3$), the conduction state at RT changed from metallic to insulating after annealing at $P(\text{O}_2) < 2 \times 10^{-3} \text{ atm}$.

No significant changes indicative of phase transition were observed in XRD patterns of the annealed samples 2–5. The $P(\text{O}_2)$ dependencies of lattice parameters a_r and α_r of LSC ($x = 0.3$) after annealing at 1073 K are shown in Fig. 6. The rhombohedral angle α_r decreased with decreasing $P(\text{O}_2)$, while the a -axis length a_r increased. The oxygen nonstoichiometry of LSC ($x = 0.3$) is sharply affected by a change in $P(\text{O}_2)$ when the sample is annealed at low $P(\text{O}_2)$ as shown in Table 1. The sample annealed and cooled at $P(\text{O}_2) = 1 \times 10^{-3} \text{ atm}$, which is insulating at RT, has many oxygen vacancies and described as $\text{La}_{0.7}\text{Sr}_{0.3}\text{CoO}_{2.94}$.

Figure 5b shows the effect of cooling rate on the electrical conductivity of LSC ($x = 0.3$) (samples 4, 6, and 7) after annealing at $T = 1073 \text{ K}$ and $P(\text{O}_2) = 2 \times 10^{-3} \text{ atm}$. At a cooling rate of 100 K h^{-1} the LSC ($x = 0.3$) sample showed metallic behavior over the whole temperature range. In contrast, when the cooling rate was faster than

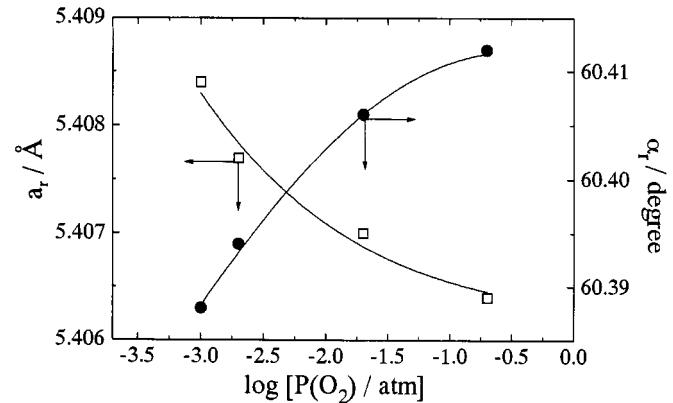


FIG. 6. Variations of (\square) a -axis length a_r and (\bullet) rhombohedral angle α_r in the rhombohedral system of $\text{La}_{0.7}\text{Sr}_{0.3}\text{CoO}_3$ after annealing at 1073 K under various $P(\text{O}_2)$ atmospheres and cooled to RT at 100 K h^{-1} .

100 K h^{-1} , MIT appeared on cooling. The MIT temperature shifted to a higher temperature with increasing cooling rate. This phenomenon can be correlated with the oxygen nonstoichiometry as shown in Table 1. During cooling oxygen is incorporated into an annealed sample accompanying the oxidation of Co^{3+} to Co^{4+} , but when the cooling rate is high, oxygen vacancies are frozen at a high temperature on cooling. The higher the cooling rate is, the more oxygen vacancies remain at RT. Sample 5, which was annealed and cooled in the $P(\text{O}_2) = 1 \times 10^{-3} \text{ atm}$ atmosphere and showed MIT on cooling, was reheated at 730 K in air (sample 9). Sample 9 showed metallic behavior ($\partial\sigma/\partial T < 0$) over the whole temperature range on cooling. Its n value was nearly equal to that of as-sintered in

TABLE 1
Mean Valence of Cobalt n and Nonstoichiometry $3-\delta$ in $\text{La}_{0.7}\text{Sr}_{0.3}\text{CoO}_{3-\delta}$ Annealed under Various Conditions

Sample	Annealing conditions				n	$3-\delta$	MIT (K)
	T (K)	$P(\text{O}_2)$ (atm)	Cooling rate (K h^{-1})				
1 ^a	1473	2×10^{-1}	100	3.22	2.96	m^b	
2	1073	2×10^{-1}	100	3.23	2.97	m^b	
3	1073	4×10^{-3}	100	3.20	2.95	m^b	
4	1073	2×10^{-3}	100	3.20	2.95	m^b	
5	1073	1×10^{-3}	100	3.18	2.94	473	
6	1073	2×10^{-3}	200	3.18	2.94	310	
7	1073	2×10^{-3}	500	3.15	2.93	373	
8	1473	1×10^{-2}	100	2.29	2.50	— ^c	
9 ^d	730	2×10^{-1}	100	3.23	2.97	m^b	

^aAs-sintered sample.

^bMetallic over the whole temperature range.

^cDecomposed.

^dSample 5 was reannealed.

air (sample 1), which shows that it had almost no oxygen vacancies. From these facts it is reasonable to say that the conduction state of LSC is dominated by the concentration of oxygen vacancies, rather than by oxygen partial pressure itself.

3.3. Variations of Interatomic Distance and Angle with x , T , and $P(O_2)$

In the rhombohedral LSC (space group: $R\bar{3}c$), only oxygen atoms (6c site) can change their positions, while La, Sr, and Co atoms are fixed at their equivalent positions (La and Sr: 2a site, Co: 2b site). The Co–O–Co angle θ is 180° in the cubic region; that is, CoO_6 forms an equilateral octahedron. In the rhombohedral region, θ is less than 180° because of oxygen displacement by tilting of adjacent CoO_6 octahedra to opposite directions with each other along each (pseudo-) cubic axis (24). Figures 7 and 8 show the variations of the Co–O distance and Co–O–Co angle, respectively, with x (19), T , and $P(O_2)$. The Co–O distance decreased with an increase in x (19) or $P(O_2)$, whereas it increased with an increase in T . In each case, a discontinuous contraction of the Co–O distance was observed at MIT, that is, at $x \sim 0.25$ (at RT in air), at $T \sim 973$ K ($x = 0.0$ in air) or at $P(O_2) \sim 2 \times 10^{-3}$ atm ($x = 0.3$ at RT). The approach of neighboring cobalt and oxygen atoms at the metallic side of each MIT is responsible for the contraction of the lattice parameter described above.

In contrast to the variations of the Co–O distance, the Co–O–Co angle θ increased with increasing each variable, x , T or $P(O_2)$; that is, whenever the conduction state changed from insulating to metallic, θ increased. At around each MIT, the change in the Co–O–Co angle was discontinuous as was observed for the Co–O distance.

4. DISCUSSION

Some intuitive models based on chemical bonding have been proposed to explain the MIT mechanism of transition-metal oxides (10, 25–27). Goodenough *et al.* (10) considered that the degree of the overlap of cation–anion or cation–anion–cation electron orbitals decides the character of d -electrons, collective or localized, in the vicinity of the Fermi level in materials with narrow d -bands. On the basis of this consideration, they introduced the concept of critical lattice parameter and suggested that materials that have lattice parameters shorter than critical ones have metallic conductivity. Goodenough *et al.*'s approach is very useful and intuitive for explaining systematically electrical and magnetic properties of many transition-metal oxides. However, the description of MIT in LSC has not been satisfactorily explained only in terms of this model.

The variations of crystallographic parameters a_r , α_r , the Co–O distance, and θ , with an increase in each variable, x ,

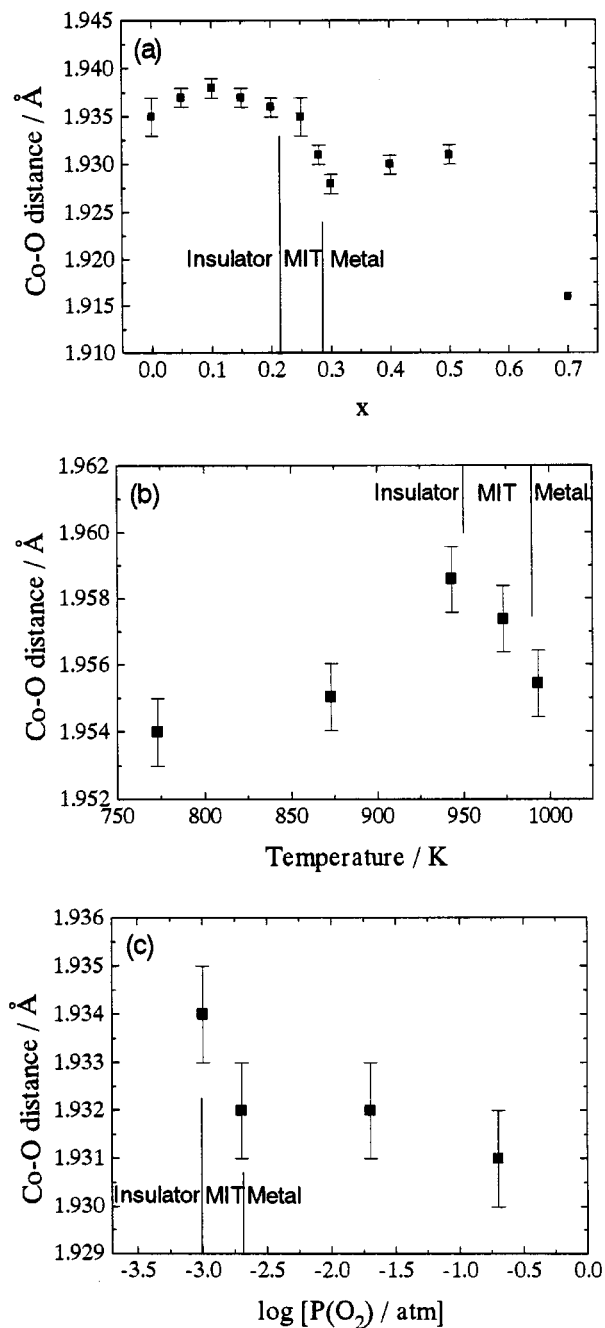


FIG. 7. Co–O distance of LSC as functions of x , T , and $P(O_2)$: (a) at RT and $P(O_2) = 2 \times 10^{-1}$ atm (19); (b) $x = 0.0$ and $P(O_2) = 2 \times 10^{-1}$ atm; (c) $x = 0.3$ and RT after annealing at 1073 K in different $P(O_2)$.

T , or $P(O_2)$, are summarized in Table 2. The conduction state changed from insulating to metallic with an increase in x , T , or $P(O_2)$; hence, Table 2 shows how these parameters change when the conduction state changed from insulating to metallic. With an increase in $P(O_2)$, a_r decreased and the conduction state changed from insulating to metallic, which is in agreement with the concept of the critical lattice

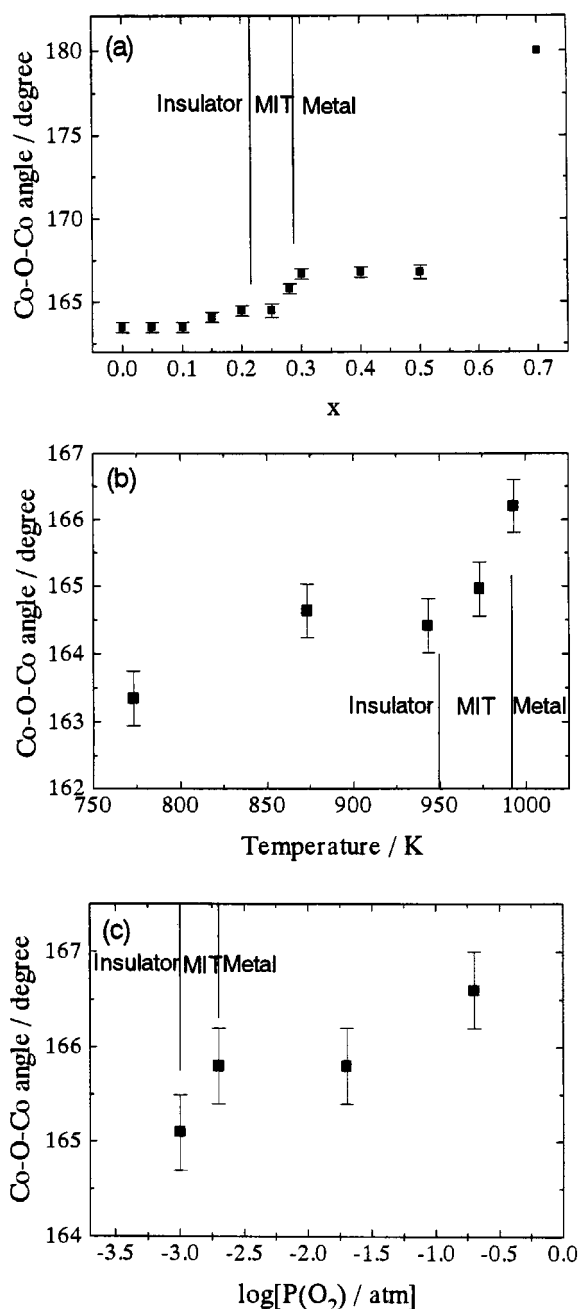


FIG. 8. Co–O–Co angle θ of LSC as functions of x , T , and $P(\text{O}_2)$: (a) at RT and $P(\text{O}_2) = 2 \times 10^{-1}$ atm (19); (b) $x = 0.0$ and $P(\text{O}_2) = 2 \times 10^{-1}$ atm; (c) $x = 0.3$ and at RT after annealed at 1073 K in different $P(\text{O}_2)$.

parameter proposed by Goodenough *et al.* However, when x or T increased, a_r increased; nevertheless, the conduction state changed from insulating to metallic. The a -axis length a_r kept increasing with x or temperature even in the metallic region although a discontinuous contraction of a_r was observed at MIT (x or T). It should be noted that no change in lattice symmetry (space group) was accompanied by MIT. Hence a subtle change in atomic configurations caused MIT

TABLE 2
Variations of Crystallographic Parameters with an Increase in Variables, x , T , or $P(\text{O}_2)$

Variable	Crystallographic parameters			
	a_r	α_r	Co–O distance	θ
x^a	↑	↓	↓	↑
T^b	↑	↓	↑	↑
$P(\text{O}_2)^c$	↓	↑	↓	↑

Note. Symbols ↑ and ↓ mean an increase and decrease of the parameter, respectively, with an increase in each variable, x , T , or $P(\text{O}_2)$. In each case, the conduction state changed from insulating to metallic when each variable, x , T , or $P(\text{O}_2)$, was increased.

^aRT and $P(\text{O}_2) = 2 \times 10^{-1}$ atm (19).

^b $x = 0.0$ and $P(\text{O}_2) = 2 \times 10^{-1}$ atm.

^c $x = 0.3$ and at RT after annealing at 1073 K in different $P(\text{O}_2)$.

of LSC. With an increase in x or $P(\text{O}_2)$, Co–O distance decreased, whereas it increased with an increase in T . In addition, the values of Co–O distance at three kinds of MITs were rather different from one another as shown in Fig. 7. These facts show that the concept of the critical lattice parameter cannot be applied directly to MIT of LSC.

The rhombohedral angle α_r decreased with increasing x or T ; that is, the symmetry of crystal was improved when the conduction state changed from insulating to metallic. On the contrary, when the conduction state became metallic by an increase in $P(\text{O}_2)$, α_r changed in the opposite direction. Hence the change in α_r does not systematically explain the variation of the conduction state, either.

In contrast to the above cases, the Co–O–Co angle θ expanded with increasing each variable, x , T , or $P(\text{O}_2)$; that is, the transition from insulator to metal is always accompanied by an increase in θ . Here a discontinuous change in θ was also observed at each MIT. It should be noted that MIT took place at $\theta \sim 165^\circ$ in each case as shown in Fig. 8. Since each MIT can be consistently discussed by crystallographic consideration using θ , the variation of θ is the most probable origin of MIT in LSC. This means that the degree of tilting in CoO_6 octahedra determines whether the conduction state is metallic or insulating.

The Co–O–Co angle or the degree of the tilting of CoO_6 octahedra should be closely related to rhombohedral distortion. From this point of view, it would be possible to consider that the degree of rhombohedral distortion dominates the conduction state. However, it is not the case for the change in $P(\text{O}_2)$ because the change in α_r showed the opposite tendency as discussed earlier. This is due to the presence of a large amount of oxygen vacancies in samples annealed at low $P(\text{O}_2)$ because not only the Co–O–Co angle but also oxygen vacancies should affect the symmetry of the crystal.

Zaanen *et al.* (28) summarized the band gaps and electronic structures of transition-metal compounds in a diagram (the so-called ZSA diagram). The ZSA diagram predicts that there are two general types of gap. One is the Mott–Hubbard gap due to the Coulomb correlation energy (U) between the d -bands of transition metal (the upper and lower Hubbard bands). The other is the charge-transfer (CT) gap due to an energy difference (Δ) between the p -band of ligand anions and the upper Hubbard band of transition metal (29). According to these two types of band gaps, insulators are classified into two groups: Mott–Hubbard insulators and CT insulators. Transition from insulator to metal occurs when the Mott–Hubbard gap or the CT gap closes; that is, the energy difference U or Δ , respectively, becomes smaller than the bandwidth (W). On the basis of their model, Torrance *et al.* (30) systematically accounted for the conduction state, metallic or insulating, for a wide variety of transition-metal oxides using a simple ionic model. They showed that LaCoO_3 is a CT insulator, which was later confirmed by soft X-ray absorption (31) and by optical reflectivity spectroscopy (32).

Torrance *et al.* (33) studied MIT in RNiO_3 ($R = \text{Pr, Nd, Sm, and Eu}$) CT insulators and concluded that transition from insulator to metal is most probably caused by the closing of the CT gap, induced by an increase in the electronic bandwidth of the occupied O-2*p* valence band and the unoccupied Ni-3*d* conduction band. They also pointed out that the Ni–O–Ni angle plays an important role in MIT since the electronic bandwidth is closely related to $\cos \theta$ (34). In this study, MIT of LSC is consistently described by the change in the Co–O–Co angle. Therefore, transition from insulator to metal of LSC takes place in a manner similar to that of RNiO_3 system.

Figure 9 shows a model showing the correlation of the electronic structure of LSC ($x = 0.0$) and the Co–O–Co angle when the temperature is raised. Insulating LSC ($x = 0.0$) has a band gap between O-2*p* and Co-3*d* bands as shown in Fig. 9a (30), where θ is less than 165° . With increasing T , the degree of tilting of CoO_6 octahedra reduces and thereby θ increases, which results in broadening of the bandwidths as shown in Fig. 9b. When the Co–O–Co angle reaches ca. 165° , the CT gap Δ becomes smaller than the bandwidth W , giving rise to a metallic state (Fig. 9c). The broadening of O-2*p* and Co-3*d* bands and resulting enhancement of their overlap cause a discontinuous contraction in the Co–O bond length and an expansion in θ at MIT. Hence, the discontinuous contraction of the lattice observed at MIT is not the origin of MIT, but can be regarded as a consequence of MIT. When T is raised further, θ becomes closer to 180° , and thereby the overlap is enhanced further (Fig. 9d) even if the Co–O distance increases with T in the case of MIT (T).

Senaris and Goodenough (35, 36) showed that Co^{3+} ions in LSC ($x = 0.0$) alter their spin state by temperature rise:

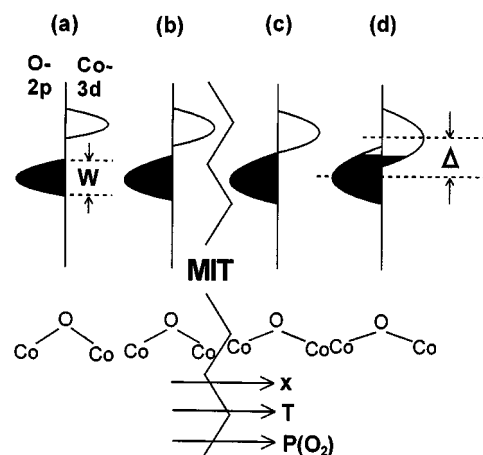


FIG. 9. Schematic model showing the correlation of the electronic structure of LSC and the Co–O–Co angle at MIT. (a, b) CT insulator region; (c, d) semimetal region. The bandwidth broadens and θ straightens out with an increase in each variable. At $\theta \sim 165^\circ$ between (b) and (c), insulator-to-metal transition takes place by overlapping of O-2*p* and Co-3*d* bands.

they are essentially all low-spin configurations at $0 < T/\text{K} < 35$, a mixture of low-spin and high-spin configurations at $110 < T/\text{K} < 350$, and a mixture of intermediate-spin and high-spin configurations at $T \geq 650 \text{ K}$, respectively. Since the electronic structure of LSC is significantly affected by the spin state of cobalt, the diagram shown in Fig. 9 should be modified somewhat to describe its exact electronic structure as a function of temperature. Senaris and Goodenough considered that the conversion of low-spin to intermediate-spin cobalt ions by temperature rise causes the transition from semiconducting to metallic [MIT(T)] (35). However, MIT(T) of LSC ($x = 0.0$) was observed at $T \sim 973 \text{ K}$; the temperature is much higher than that for the spin conversion. In addition, no spin conversion was reported at MIT(T). Hence, it is reasonable to think that the expansion in θ causes MIT(T) with an increase in the electronic bandwidth regardless of the spin state of cobalt.

In cases of MIT(x) and MIT(P), the presence of doped states introduced by Sr doping and oxygen vacancies should be considered, and they may change the electronic structure significantly. In addition, Raccach *et al.* (11) pointed out that segregation of LSC may take place upon doping of Sr. Senaris and Goodenough (36) described that LSC segregates into hole-rich (metallic and ferromagnetic) regions, which are created by Sr doping, and a hole-poor matrix similar to LSC ($x = 0.0$). They considered that when the coupling between the hole-rich regions reaches a magnetic percolation threshold, LSC undergoes the transition from semiconducting to metallic [MIT(x)]. However, no evidence indicative of such segregation was seen in the XRD patterns in the present study.

In the present study, θ is the only parameter that consistently describes the change in the conduction state of LSC by a change in each variable, and the conduction state changed from insulating to metallic at $\theta \sim 165^\circ$, as was observed for MIT(T). These facts indicate that the three MITs can be systematically explained by the model in Fig. 9; that is, the increase in the electronic bandwidth is the most probable origin of MIT for each case [MIT(x , T , or P)].

5. CONCLUSIONS

We studied the electrical conductivity and crystal structure of $\text{La}_{1-x}\text{Sr}_x\text{CoO}_3$ as functions of three variables [x , T , and $P(\text{O}_2)$] and found that MIT appears by a change in $P(\text{O}_2)$ as well as x and T . The variations of crystallographic parameters, a_r , α_r , the Co–O distance, and θ , were determined using an X-ray powder Rietveld method. The Co–O–Co angle, that is, the degree in the tilting of CoO_6 octahedra, is the only parameter that consistently describes MIT caused by a change in each variable, x , T or $P(\text{O}_2)$. In each case, θ increased when the conduction state changed from insulating to metallic, and MIT(x , T , or P) appeared when the Co–O–Co angle reached a critical value of $\theta \sim 165^\circ$. From these facts, we concluded that the transition from insulator to metal of LSC is caused by the closing of the charge-transfer gap, which is induced by broadening of the electronic bandwidth of the Co-3d and O-2p bands.

ACKNOWLEDGMENTS

Computation time for Rietveld refinements was provided by the Super-computer Laboratory, Institute for Chemical Research, Kyoto University. This work was supported by Grant-in-Aids for Scientific Research (No. 07239105) from the Ministry of Education, Science, Sports, and Culture, Japan.

REFERENCES

- C. S. Tedmon Jr., H. S. Spacil, and S. P. Mitoff, *J. Electrochem. Soc.* **116**, 1170 (1969).
- N. Q. Minh, *J. Am. Ceram. Soc.* **76**, 563 (1993).
- H. Yokokawa, N. Sakai, T. Kawada, and M. Dokiya, *J. Electrochem. Soc.* **138**, 2719 (1991).
- H. U. Anderson, *Solid State Ionics* **52**, 33 (1992).
- O. Yamamoto, Y. Takeda, N. Imanishi, and Y. Sakaki, in "Proceedings of the 3rd International Symposium on Solid Oxide Fuel Cells" (S. C. Singhal and H. Iwahara, Eds.), p. 205. The Electrochemical Society, Pennington NJ, 1993.
- S. Carter, A. Selcuk, R. J. Chater, J. Kajda, J. A. Kilner, and B. C. H. Steele, *Solid State Ionics* **53–56**, 597 (1992).
- B. A. van Hassel, T. Kawada, N. Sakai, H. Yokokawa, M. Dokiya, and H. J. M. Bouwmeester, *Solid State Ionics* **66**, 295 (1993).
- Y. Teraoka, H. Zhang, S. Furukawa, and N. Yamazoe, *Chem. Lett.*, 1743 (1985).
- G. H. Jonker and J. H. Van Santen, *Physica* **19**, 120 (1953).
- P. M. Raccach and J. B. Goodenough, *Phys. Rev.* **155**, 932 (1967).
- P. M. Raccach and J. B. Goodenough, *J. Appl. Phys.* **39**, 1209 (1968).
- V. G. Bhide, D. S. Rajoria, C. N. R. Rao, G. Rama Rao, and V. G. Jadhao, *Phys. Rev. B* **12**, 2832 (1975).
- P. L. Gai and C. N. R. Rao, *Mater. Res. Bull.* **10**, 787 (1975).
- G. Thornton, B. C. Tofield, and A. W. Hewat, *J. Solid State Chem.* **61**, 301 (1986).
- G. Thornton, F. C. Morrison, S. Partington, B. C. Tofield, and D. E. Williams, *J. Phys. C* **21**, 2871 (1988).
- J. Mizusaki, J. Tabuchi, T. Matsuura, S. Yamauchi, and K. Fueki, *J. Electrochem. Soc.* **136**, 2082 (1989).
- J. P. Kemp, D. J. Beal, and P. A. Cox, *J. Solid State Chem.* **86**, 50 (1990).
- H. Eisaki, T. Ido, K. Magoshi, M. Mochizuki, H. Yamatsu, T. Ito, and S. Uchida, *Physica C* **185–189**, 1295 (1991).
- A. Mineshige, M. Inaba, T. Yao, Z. Ogumi, K. Kikuchi, and M. Kawase, *J. Solid State Chem.* **121**, 423 (1996).
- T. Yao, "Report of Grand-in-Aid for Scientific Research (No. 02650560) from the Ministry of Education, Science and Culture, Japan," p. 34, 1992.
- Y. Teraoka, H. M. Zhang, K. Okamoto, and N. Yamazoe, *Mater. Res. Bull.* **23**, 51 (1988).
- C.H. Chen, H. J. M. Bouwmeester, R. H. E. van Doorn, H. Kruidhof, and A. J. Burggraaf, *Solid State Ionics* **98**, 7 (1997).
- Y. Ohno, S. Nagata, and H. Sato, *Solid State Ionics* **9/10**, 1001 (1983).
- A. M. Glazer, *Acta Crystallogr. B* **28**, 3384 (1972).
- C. N. R. Rao and G. V. S. Rao, *Phys. Stat. Sol. (a)* **1**, 597 (1970).
- J. B. Goodenough, in "Progress in Solid State Chemistry" (H. Reiss, Ed.), Chapter 4, Pergamon, Oxford, 1971.
- N. F. Mott, *Proc. R. Soc. Lond. A* **382**, 1 (1982).
- J. Zaanen, G. A. Sawatzky, and J. W. Allen, *Phys. Rev. Lett.* **55**, 418 (1985).
- S. Hüfner, *Solid State Commun.* **49**, 1177 (1984).
- J. B. Torrance, P. Lacorre, C. Asavaroengchai, and R. M. Metzger, *Physica C* **182**, 351 (1991).
- D. D. Sarma, A. Chainani, R. Cimino, P. Sen, C. Carbone, M. Mathew, and W. Gudat, *Europhys. Lett.* **19**, 513 (1992).
- T. Arima, Y. Tokura, and J. B. Torrance, *Phys. Rev. B* **48**, 17006 (1993).
- J. B. Torrance, P. Lacorre, A. I. Nazzari, E. J. Ansaldo, and Ch. Niedermayer, *Phys. Rev. B* **45**, 8209 (1992).
- G. A. Sawatzky, W. Geertsma, and C. Haas, *J. Magn. Magn. Mater.* **3**, 37 (1976).
- M. A. Senaris-Rodriguez and J. B. Goodenough, *J. Solid State Chem.* **116**, 224 (1995).
- M. A. Senaris-Rodriguez and J. B. Goodenough, *J. Solid State Chem.* **118**, 323 (1995).